Evaluation of exchange-correlation functionals with multiple-shock conductivity measurements in hydrogen and deuterium at the molecular-to-atomic transition

M. D. Knudson*
Institute for Shock Physics, Washington State University, Pullman, Washington 99164, USA

M. P. Desjarlais
Sandia National Laboratories, Albuquerque, New Mexico 87185-1195, USA

M. Preising and R. Redmer
Institute of Physics, University of Rostock, Rostock, Germany

(Received 16 August 2018; published 26 November 2018)

The temperature (T) and density (ρ) conditions at which hydrogen undergoes a molecular-to-atomic (MA) transition is crucial to our understanding of the gas-giant planets such as Jupiter and Saturn. First-principles (FP) calculations suggest that this transition is coincident with metallization and acts as a catalyst for hydrogen-helium demixing, which has significant consequences for models of planetary interiors. Prediction of this transition boundary has proven to be difficult using FP methods. In particular, detailed comparisons of finite temperature density functional theory (FT-DFT) calculations of the MA transition in both the high-T, low-ρ regime, where the transition is largely T driven, and the low-T, high-ρ regime, where the transition is largely ρ driven, suggest that the transition is very sensitive to the exchange-correlation (xc) functional used in the calculation. Here we present a detailed comparison of previous multiple-shock electrical conductivity measurements with FT-DFT calculations employing various xc functionals to probe a regime where both T and ρ play an important role in the transition. The measurement results are found to be inconsistent with the semilocal xc functional PBE and are in much better agreement with the nonlocal xc functionals vdW-DF1 and vdW-DF2. Furthermore, we show that the inconsistency with PBE likely stems from pressure errors associated with the PBE xc functional, resulting in calculated pressures that are too low at these T and ρ conditions. Together with previous comparisons at high-T, low-ρ and low-T, high-ρ these results provide a consistent picture for the MA transition over a wide T and ρ range. This picture may also provide insight into differences in experimental observations of the metallization of liquid hydrogen and deuterium in the low-T regime.

DOI: 10.1103/PhysRevB.98.174110

I. INTRODUCTION

The question of precisely how and at what pressure (P) hydrogen metallizes at low temperature (T) has become one of the longest-standing open questions of high-pressure physics [1]. Also of great interest, due to its relevance to planetary science [2,3], is the analogous molecular insulator to atomic metal transition in the liquid at low T, just above the melt boundary. First-principles (FP) calculations suggest that hydrogen metallization is coincident with a molecular-to-atomic (MA) transition and acts as a catalyst for hydrogen-helium demixing [4]. Thus the location of the MA transition in the low-T liquid could provide a constraint for the low-P boundary of the region of hydrogen-helium immiscibility and justification for the presence of a layer boundary in the interior of gas-giant planets, a necessary feature of the often-used three-layer model [5], which has shown reasonable success in describing observables of Jupiter and Saturn [6].

Hydrogen, as one of the simplest elemental systems, has also been a model system in the development of advanced FP simulation techniques including finite temperature density functional theory (FT-DFT) and quantum Monte Carlo (QMC) methods [1]. However, prediction of the MA transition using FP methods has proven to be very sensitive to the framework used. Recent work [7] comparing FT-DFT methods to the deuterium Hugoniot—the locus of end states achievable through compression by large amplitude shock waves—concluded that no one exchange-correlation (xc) functional adequately describes the MA transition. In this high-T (∼5–10 kK), low-density (ρ) regime where dissociation is largely T driven the P onset of the MA transition, as evidenced by first-shock ρ and reshock P measurements, is underestimated by the semilocal xc functional PBE [8] and is best described by nonlocal functionals, such as vdW-DF1 [9] and vdW-DF2 [10]. However, the P width over which dissociation occurs is likely overestimated by these vdW functionals and is in better agreement with PBE.

Differences between functionals become even more pronounced in the low-T (∼1–2 kK), high-ρ regime where the MA transition appears to be largely ρ driven. In this regime the predicted transition P and ρ are extremely sensitive to

*Present address: Sandia National Laboratories, Albuquerque, New Mexico 87185-1195, USA; mdknuds@sandia.gov

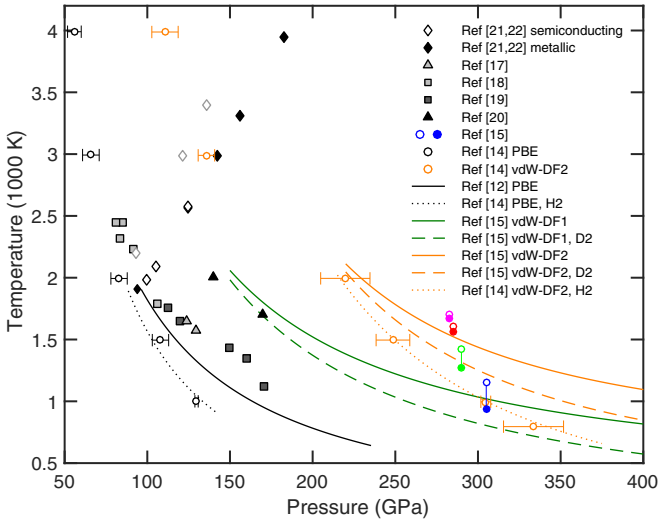

FIG. 1. T-P phase diagram showing experimental and theoretical estimates for the metallization of hydrogen/deuterium. Experiment: open (closed) diamonds [21,22], semiconducting (metallic) states from multiple-shock experiments with corrected T (see Sec. II); gray triangle [17], gray square [18], black square [19], and black triangle [20], static high-P and pulsed heated experiments; colored open and closed circles [15], dynamic compression experiments. Theory: open black (orange) circles [14], calculations of $\sigma = 2000\ (\Omega\ \mathrm{cm})^{-1}$ for PBE (vdW-DF2) with nuclear (hydrogen) treatment for the ions; solid [12] and dotted [14] black lines, first-order MA transition boundary for PBE with classical and nuclear (hydrogen) treatment for the ions, respectively; solid and dashed green lines [15], transition boundary for vdW-DF1 with classical and nuclear (deuterium) treatment for the ions, respectively; solid [15], dotted [14], and dashed [15] orange lines, transition boundary for vdW-DF2 with classical, nuclear (hydrogen), and nuclear (deuterium) treatment of the ions, respectively.

the xc functional. For PBE, vdW-DF1, and vdW-DF2 the predicted transition P differs by ∼200–300 GPa (see Fig. 1) and the ρ at the transition ranges from ∼0.75–1.2 g/cm^3 for hydrogen and ∼1.5–2.4 g/cm^3 for deuterium [11–15]. Experimental determination of the MA transition in this regime also spans a large range in P. Dynamic compression experiments [15] on liquid deuterium in the ∼1–2 kK regime performed at the Sandia Z machine [16] revealed an abrupt MA transition, as evidenced by a sudden increase in reflectivity between ∼280 and 305 GPa, in reasonable agreement with the nonlocal vdW-DF2 xc functional. Static high-P and pulsed heated experiments [17–20] on hydrogen and deuterium in a similar T regime suggest the MA transition occurs at ∼75 to 170 GPa, based on observation of T plateaus in the heating curves and increases in reflectivity, seemingly in better agreement with the semilocal xc functional PBE.

The first experiments [21,22] to address the MA transition in liquid hydrogen and deuterium were performed roughly 20 years ago using gas-gun techniques. In that study multiple-shock compression, achieved through a wave reverberation technique, was used to attain successively higher P and T states in liquid hydrogen and deuterium. Measurement of the electrical conductivity (σ) in the peak state revealed saturation at ∼2000 $(\Omega\ \mathrm{cm})^{-1}$, a value consistent with minimum metallic conductivity, at a P of ∼140 GPa and an estimated T of ∼2600 K. This set of experiments provides another very good test of FP methods in a regime in which both T and ρ (or P) play an important role in the MA transition. However, while indirect comparisons between the measured σ and FP calculations have been made, to the best of our knowledge no one has performed a detailed comparison of these experimental results with FP calculations.

Here we present a detailed comparison of the measured σ from multiple-shock compression experiments [21,22] with FT-DFT calculations using both semilocal (PBE) and nonlocal (vdW-DF1 and vdW-DF2) xc functionals. We show that the measured results are inconsistent with PBE predictions. Similar to both the T-driven and ρ-driven regime, PBE appears to underestimate the P conditions necessary for dissociation. In contrast, the MA transition appears to be better described by the vdW xc functionals. Furthermore, we show that the inconsistency with PBE likely stems from P errors associated with the PBE xc functional, resulting in calculated P that are too low at these T and ρ conditions. These results, along with the previous studies comparing the various xc functionals in the T-driven [7] and ρ-driven [15] regimes, provide a consistent picture for the MA transition over a wide P and T range and raise questions about the recent static high-P and pulsed heated studies [17–20] that appear to be in agreement with predictions from PBE.

Section II summarizes the multiple-shock experiments [21,22] and includes a reanalysis of the results. The original study included inconsistencies in both the inferred T states reached and in the fit to a semiconductor model used to interpret the measured σ. Correction of both of these inconsistencies is important with respect to comparisons with the FP calculations. Section III describes the FT-DFT calculations performed to determine σ and the energy gap for the various xc functionals and compares these with the experimental measurements. The results are discussed in Sec. IV. The main findings are summarized in Sec. V.

II. REANALYSIS OF MULTIPLE-SHOCK CONDUCTIVITY EXPERIMENTS

The first experiments [21,22] to address the MA transition in hydrogen and deuterium were performed roughly 20 years ago by Nellis, Weir, and Mitchell (NWM) using gas-gun techniques. A layer of liquid hydrogen or deuterium was compressed by multiple shocks using a wave reverberation technique; this minimized the entropy increase, thereby minimizing the temperature (T) in the peak state. The sample was contained within a cell between two sapphire anvils and cooled to cryogenic temperatures. The sample cell was impacted by a metal anvil (either aluminum or copper) resulting in a strong shock wave that reverberated between the relatively stiff sapphire anvils, driving the sample to high pressure (P) and density (ρ) and relatively low T. The impact velocity (v_f) was measured using a flash x-ray technique [23]. The peak P of the sample was determined from the known equations of state (EOS) of aluminum, copper, and sapphire and the measured v_f (in the reverberation configuration the peak P is only a function of the confining anvils and does not depend upon the EOS of hydrogen or deuterium). The electrical

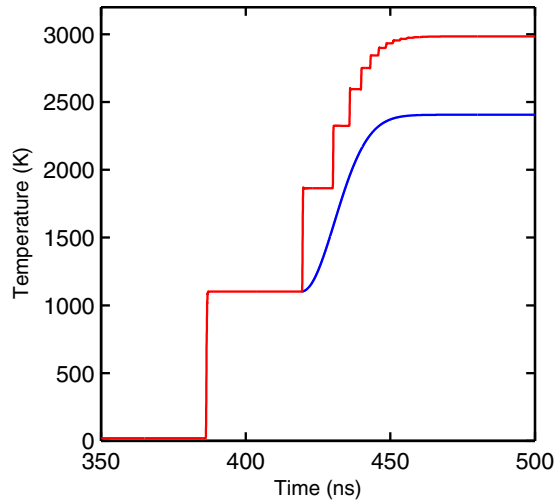

FIG. 2. Comparison of the two methods used by NWM to infer T in the multiple-shock experiments on hydrogen and deuterium. Red line: hydrodynamic simulation accounting for the full multiple-shock nature of the experiment (in this case SLDMS12-H_2). Blue line: hydrodynamic simulation with the same magnitude first shock followed by ramp compression to the same peak P (in this case 142 GPa). Both simulations used the Kerley03 [28] EOS for hydrogen (a modern revision of the Kerley [24] EOS used by NWM).

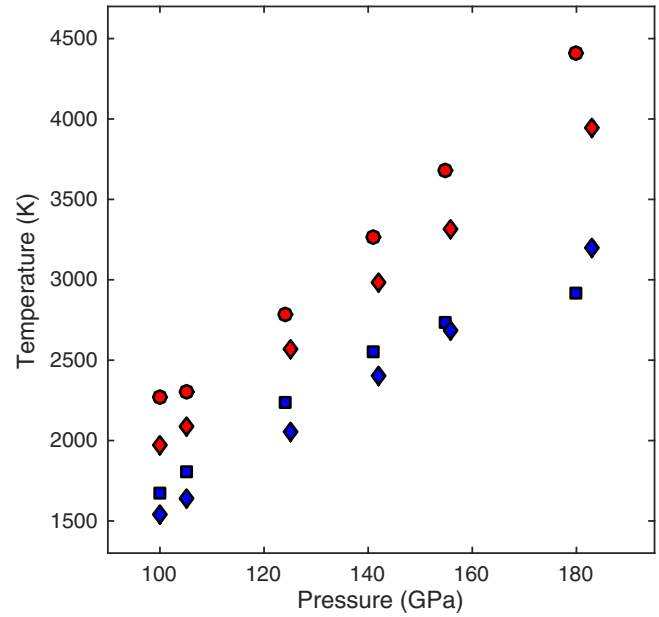

FIG. 3. Comparison of the inferred T for the NWM hydrogen experiments. The colors and symbols denote the method used to infer T and the EOS model, respectively: Red and blue correspond to method 1 and 2, respectively; squares, circles, and diamonds correspond to the Ross [25–27], Kerley [24], and Kerley03 [28] EOS, respectively.

conductivity (σ) was measured at the peak state using either a constant-voltage, two-probe method [$\sigma < 10\ (\Omega\ \mathrm{cm})^{-1}$] or a constant-current, four-probe method [$\sigma > 10\ (\Omega\ \mathrm{cm})^{-1}$]. We note that v_f and σ were the only quantities measured in these experiments.

To estimate the T and ρ of the sample in the peak state two different EOS models for hydrogen and deuterium were considered; a tabular EOS denoted as Kerley [24] and an analytical EOS denoted as Ross [25–27]. Because only one of these EOS models (Kerley) was in a tabular format, conducive for use in hydrodynamic simulations, two different methods were used to infer T and ρ; these two methods were described by NWM as being different but equivalent. Method 1, used for the Kerley EOS, inferred T and ρ from hydrodynamic simulations of the impact experiments and therefore fully accounted for the multiple-shock nature of the experiments. Method 2, used for the Ross EOS, inferred T and ρ by determining $T(P_{\mathrm{max}})$ and $\rho(P_{\mathrm{max}})$ along an isentrope centered at the first shocked state of the hydrogen or deuterium (P_1, T_1, and ρ_1), where P_{max} was the peak P reached in the experiment. In other words, method 2 only accounted for the entropy increase due to the first shock and treated the subsequent compression as isentropic.

These two methods are, in fact, not equivalent; method 2 fails to account for the non-negligible increase in entropy that results from the subsequent shocks during the reverberation. The difference in these two methods is illustrated in Fig. 2, which shows two different hydrodynamic simulations using the same EOS for hydrogen, Kerley03 [28], a modern revision of the Kerley EOS used by NWM. The red line represents a simulation accounting for the full multiple-shock nature of the experiment (method 1). The blue line represents a simulation with the same magnitude first shock followed by ramp compression to the same peak P (method 2). In these simulations EOS models 3325 [29,30], 3700 [31,32], and 7411 [33] were used to model copper, aluminum, and sapphire, respectively. As can be seen in the figure, T in the peak state for these two simulations differs by over 500 K. This is completely explained by the difference in entropy of the final states for the two different methods used by NWM. As a result, the T in the peak states inferred by NWM using the Kerley EOS with method 1 and the Ross EOS with method 2 were considerably different.

The differences in inferred T for the subset of hydrogen experiments performed by NWM are shown graphically in Fig. 3 and listed in Table I. The colors and symbols denote the method used to infer T and the EOS model, respectively: Red and blue correspond to method 1 and 2, respectively; squares, circles, and diamonds correspond to the Ross, Kerley, and Kerley03 EOS, respectively. As can be seen in Fig. 3 the largest difference in inferred T is due to the method used, not the EOS model. In particular, the red and blue diamonds represent inferred T for the same EOS model (Kerley03) using the two different methods outlined above. The T difference ranges from ∼440–750 K (∼20–30%) with an average T difference of ∼550 K over the entire P range. In contrast, differences in inferred T between various models for the same calculation method are noticeably smaller.

NWM interpreted the large T difference arising from the two calculation methods as being due to differences in the Kerley and Ross EOS models with respect to dissociation. They concluded that the Kerley EOS neglected dissociation at the conditions reached in their experiments and therefore resulted in higher inferred T as compared to the Ross EOS. They therefore chose to use the T and ρ values inferred from the Ross EOS (using method 2) to estimate the states reached

TABLE I. Inferred P, T, and ρ states reached in the multiple-shock experiments [21,22] on hydrogen and deuterium performed by NWM. The first four columns list the experiment designation, impactor material, measured impact velocity, and measured σ, respectively. The subsequent columns list the inferred P, T, and ρ reported by NWM (using the Ross EOS and method 2) and the inferred P, T, and ρ obtained using method 1 and the Kerley03 [28] and Saumon [34] EOS. The subsequent analysis performed in this work uses the values inferred from the Kerley03 EOS.

				NWM			Kerley03			Saumon		
Experiment	Impactor	v_f (km/s)	σ $(\Omega\ \mathrm{cm})^{-1}$	P (GPa)	T (K)	ρ (g/cm^3)	P (GPa)	T (K)	ρ (g/cm^3)	P (GPa)	T (K)	ρ (g/cm^3)
SLDMS4-D_2	Aluminum	5.59	0.71	93	2090	1.17	93	2204	1.25	93	2197	1.26
SLDMS5-D_2	Aluminum	6.76	77	121	2760	1.29	121	2987	1.38	121	2998	1.39
SLDMS8-D_2	Aluminum	7.33	417	135	3090	1.35	136	3397	1.44	136	3476	1.45
SLDMS6-H_2	Aluminum	5.90	2.6	100	1670	0.61	100	1978	0.64	100	1867	0.66
SLDMS13-H_2	Aluminum	6.10	7.1	105	1810	0.62	105	2093	0.66	105	1976	0.67
SLDMS7-H_2	Aluminum	6.90	135	124	2230	0.66	125	2567	0.70	125	2430	0.72
SLDMS9-H_2	Aluminum	6.91	313	124	2230	0.66	125	2573	0.70	125	2436	0.72
SLDMS12-H_2	Copper	5.58	2380	141	2560	0.69	142	2984	0.73	142	2889	0.76
SLDMS10-H_2	Copper	5.96	1670	155	2730	0.72	156	3310	0.76	156	3253	0.79
SLDMS11-H_2	Copper	6.65	2000	180	2910	0.77	183	3951	0.81	183	3848	0.84

in their experiments. However, due to the error in method 2, these conditions do not accurately reflect the T states reached. We contend that the T obtained by method 1 using the Kerley03 EOS are a better representation. We note that a similar analysis performed with a revised EOS for hydrogen and deuterium by Saumon [34] resulted in very similar T and ρ states (see Table I), lending confidence in these inferred values. Also, we note that Kerley03 is a widely-used EOS model and was used to infer T and ρ (along with the vdW-DF2 xc functional) in the low-T, high-ρ metallization study [15]. Finally, we acknowledge that EOS models based on FT-DFT calculations are available [35,36]. However, at the P, T, and ρ conditions relevant here these models rely primarily on FT-DFT calculations using the PBE [8] xc functional. As shown here and elsewhere [1,7], PBE systematically underestimates the P conditions necessary for dissociation, which can result in isentropes that exhibit $-dT/dP$ at P below where saturation in σ was observed in the NWM experiments. Perhaps even more problematic, we show in Sec. IV that PBE exhibits P errors that results in a calculated P that is too low at a given T and ρ condition, or equivalently, a ρ that is too high at a given P and T condition. For these reasons we do not consider these PBE based EOS tables in estimating the conditions reached in the NWM experiments.

To infer an energy gap as a function of ρ from their measurements of σ, NWM appealed to a simplified semiconductor model. The data were fit to

$$\sigma = \sigma_0 \exp[-E_g(\rho)/2k_BT], \tag{1}$$

where σ_0 is the limiting value of conductivity, k_B is Boltzmann's constant, and $E_g(\rho)$ is the energy gap, assumed to be linear in ρ and independent of T. The result of a least-squares fit was reported to be

$$E_g(\rho) = 20 - 62.6\rho, \tag{2}$$

where E_g is in units of eV, ρ is the molar density in units of mol/cm^3, and $\sigma_0 = 90\ (\Omega\ \mathrm{cm})^{-1}$. NWM suggested this fit was reasonable, noting that a value of $\sigma_0 = 200$–$300\ (\Omega\ \mathrm{cm})^{-1}$ is typical of liquid semiconductors. However, this value for the limiting conductivity requires a negative energy gap to reproduce the measured σ for molar densities above $\sim$0.32 mol/cm^3 (using the Ross EOS and method 2 to infer ρ), which is inconsistent with the requirement that $E_g \geqslant 0$. If one uses the same model but instead constrains σ_0 to be the average of the measured σ at saturation, $\sigma_0 = 1850\ (\Omega\ \mathrm{cm})^{-1}$, a physically reasonable result is obtained. In this case

$$E_g(\rho) = 18.3 - 49.8\rho \tag{3}$$

and the gap closes at $\sim$0.37 mol/cm^3 (using the Kerley03 EOS and method 1 to infer ρ), consistent with the observed saturation in σ.

These two fits are displayed graphically in Fig. 4(a). The black and gray circles are the energy gap values obtained from Eq. (1) using the T and ρ values inferred from the Ross EOS using method 2 and the T and ρ values inferred from the Kerley03 EOS using method 1, respectively. The dashed and solid black lines are the corresponding fits [Eq. (2) and Eq. (3), respectively]. The dashed gray line denotes the temperature of the system in eV (k_BT as a function of ρ). This figure clearly shows the inconsistent behavior that arises from setting the limiting conductivity value at $\sigma_0 = 90\ (\Omega\ \mathrm{cm})^{-1}$. The estimated energy gap reaches a value equal to (k_BT) at $\sim$0.32 mol/cm^3, significantly lower than the ρ at which a minimum metallic conductivity was reached in the experiments. In order to match the measured σ at higher ρ a negative energy gap is required. The more reasonable value of $\sigma_0 = 1850\ (\Omega\ \mathrm{cm})^{-1}$ results in an energy gap that is systematically larger by $\sim$2 eV, reaching zero at $\sim$0.37 mol/cm^3, in agreement with observations.

We note that ρ was not measured in the experiments performed by NWM; the quantity in the peak state that was most tightly constrained is the peak P. We therefore also considered the inferred energy gap as a function of P, as shown in Fig. 4(b). Again, the estimated energy gap using the T and ρ values inferred by NWM using $\sigma_0 = 90\ (\Omega\ \mathrm{cm})^{-1}$ is systematically low, reaching a value equal to (k_BT) at $\sim$120 GPa, roughly 20 GPa lower than the P at which a minimum

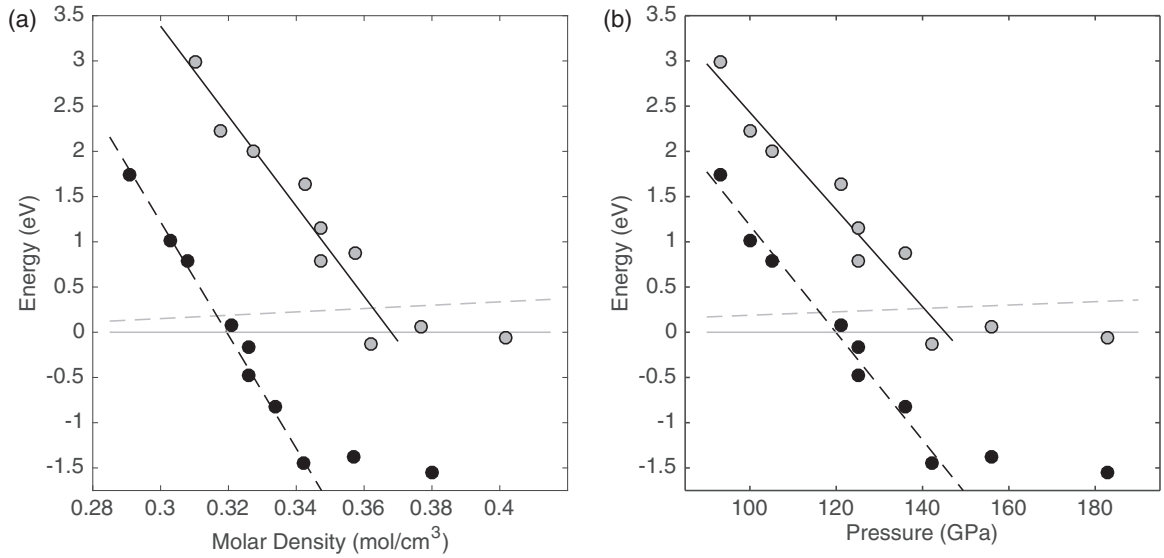

FIG. 4. Energy gap as a function of (a) molar density and (b) P. The black and gray circles are the energy gap values obtained from Eq. (1) using $\sigma_0 = 90\ (\Omega\ \mathrm{cm})^{-1}$ with T and ρ values inferred from the Ross [25–27] EOS using method 2 and those obtained from Eq. (1) using $\sigma_0 = 1850\ (\Omega\ \mathrm{cm})^{-1}$ with T and ρ values inferred from the Kerley03 [28] EOS using method 1, respectively. The dashed and solid black lines are the corresponding fits [Eq. (2) and Eq. (3), respectively]. The dashed gray line denotes the temperature of the system in eV ($k_B T$ as a function of ρ or P).

metallic conductivity was reached in the experiments. However, because of the difference in inferred ρ between the Ross and Kerley03 EOS, the systematic difference in the energy gap when viewed as a function of P is ∼1 eV. Thus the error in the NWM fit to the semiconductor model [with $\sigma_0 = 90\ (\Omega\ \mathrm{cm})^{-1}$] underestimates the energy gap by ∼1 eV as a function of P as compared to the same semiconductor model with a more reasonable value of σ_0. In the subsequent section we will compare the results of first-principles simulations to this semiconductor model.

III. COMPARISON WITH FIRST-PRINCIPLES CALCULATIONS

First-principles (FP) calculations of the electrical conductivity (σ) and the energy gap at conditions consistent with the multiple-shock compression experiments [21,22] performed by NWM were carried out within the framework of finite temperature density functional theory (FT-DFT). Both semilocal (PBE [8]) and nonlocal (vdW-DF1 [9] and vdW-DF2 [10]) exchange and correlation (xc) functionals were considered. FP molecular dynamics simulations were performed using the Vienna *ab initio* simulation package (VASP), a plane-wave DFT code developed at the Technical University of Vienna [37–39]. The density was fixed by the total volume of the cubic supercell and the ion temperature was regulated with a Nosé-Hoover thermostat [40–42]. A total 256 atoms were included in the supercell, with a plane-wave cutoff energy of 1200 eV. Simulations were performed in the canonical ensemble and typically covered a few to several picoseconds of real time. The thermodynamic quantities were taken as averages over an equilibrated portion of the cumulative averages.

The electrical conductivity was calculated by averaging over 40 randomly selected snapshots for a given temperature (T) and density (ρ) configuration using the Kubo-Greenwood [43,44] formula

$$\sigma(\omega) = \frac{2\pi e^2}{3Vm_e^2\omega} \sum_{\mathbf{k}\nu\mu} |\langle \mathbf{k}\nu|\hat{\mathbf{p}}|\mathbf{k}\mu\rangle|^2 (f_{\mathbf{k}\nu} - f_{\mathbf{k}\mu})\delta(E_{\mathbf{k}\mu} - E_{\mathbf{k}\nu} - \hbar\omega), \quad (4)$$

where ω is the frequency, V is the volume of the supercell, e and m_e are the charge and mass of electrons, respectively, and $f_{\mathbf{k}\mu}$ is the Fermi occupation number for a given temperature. The eigenvalues $E_{\mathbf{k}\mu}$ for the Bloch states $|\mathbf{k}\mu\rangle$ are computed within each step of the FT-DFT simulation so that the dipole matrix elements $\langle \mathbf{k}\nu|\hat{\mathbf{p}}|\mathbf{k}\mu\rangle$ are determined with the momentum operator. The imaginary part of the electrical conductivity can be obtained from a Kramers-Kronig transformation. For these calculations the Brillouin zone was sampled by a $5 \times 5 \times 5$ Monkhorst-Pack $\mathbf{k}$-point grid [45].

The density of states (DOS) was obtained from the same set of 40 randomly selected snapshots. For each given T and ρ configuration a histogram of the eigenvalues of the band energies was created from the collection of snapshots and smoothed with a gaussian of width 0.2 eV. The energy gaps were extracted directly from the simulations. For each time step eigenvalues in the vicinity of the fermi energy were extracted. These eigenvalues were then averaged. The energy gap was obtained from the energy difference of the averaged eigenvalues. The precision to which the energy gap can be directly computed from the simulations is set by the local separation of eigenvalue energies on either side of the gap. Eigenvalue averages for adjacent eigenstates indicate these local differences to be ∼0.15 eV; states with energy gap values on the order of 0.15 eV or less were assumed to have a closed gap and the energy gap was set to zero.

As described in Sec. II, the measured quantities in the multiple-shock experiments of NWM were the impact velocity (v_f) and σ. The peak P in the experiment was

TABLE II. Predicted σ from various xc functionals for the estimated P, T, and ρ states reached in the multiple-shock experiments [21,22] on hydrogen and deuterium performed by NWM. The first two columns list the experimental designation and the measured σ, respectively. The next three columns list the T, P, and ρ states reached as inferred using the Kerley03 [28] EOS. The subsequent columns list the predicted σ and ρ at the inferred P and T for the PBE, vdW-DF1, and vdW-DF2 xc functionals.

		Kerley03			PBE		DF1		DF2	
Experiment	σ $(\Omega\ \mathrm{cm})^{-1}$	P (GPa)	T (K)	ρ (g/cm^3)	σ $(\Omega\ \mathrm{cm})^{-1}$	ρ (g/cm^3)	σ $(\Omega\ \mathrm{cm})^{-1}$	ρ (g/cm^3)	σ $(\Omega\ \mathrm{cm})^{-1}$	ρ (g/cm^3)
SLDMS4-D_2	0.71	93	2204	1.25	4989	1.397	1.99	1.249	0.30	1.222
SLDMS5-D_2	77	121	2987	1.38	8919	1.534	4518	1.437	493	1.359
SLDMS8-D_2	417	136	3397	1.44	9970	1.589	5461	1.514	3234	1.455
SLDMS6-H_2	2.6	100	1978	0.64	3456	0.710	0.62	0.641	0.11	0.624
SLDMS13-H_2	7.1	105	2093	0.66	4990	0.729	2.32	0.652	0.35	0.636
SLDMS7-H_2	135	125	2567	0.70	9034	0.780	1546	0.722	16.2	0.683
SLDMS9-H_2	313	125	2573	0.70	9034	0.781	1546	0.722	16.2	0.683
SLDMS12-H_2	2380	142	2984	0.73	10410	0.816	5671	0.777	1693	0.737
SLDMS10-H_2	1670	156	3310	0.76	11290	0.840	7061	0.807	3880	0.774
SLDMS11-H_2	2000	183	3951	0.81	13180	0.881	8907	0.854	6551	0.827

determined from the measured v_f and the known EOS of the impactor (copper or aluminum), baseplate (aluminum), and anvils (sapphire). In the reverberation geometry used in these experiments the P in the peak state is independent of the EOS of hydrogen or deuterium and is therefore well constrained. In contrast, T and ρ in the peak state are calculated and are therefore dependent upon the particular model used for hydrogen or deuterium. For the reasons discussed in Sec. II, we used the Kerley03 [28] EOS to estimate the T and ρ conditions at the corresponding peak P (see Table II).

To perform a detailed comparison of the NWM experiments with FP calculations we first had to determine how best to equate the peak state of the system. In general, the EOS surfaces of different models are not coincident. Thus, in comparing two models one can only match two of the three variables P, T, and ρ that define a particular state of the system. Since the peak P in these experiments does not depend upon the hydrogen or deuterium EOS, P is an obvious choice for one of the variables to equate. The second variable to equate is less obvious. However, in exploring the EOS surface it was found that in this P, T, and ρ regime P depends much more strongly on ρ than T. For example, at ~100 GPa a ~10% increase in P required only a ~5% increase in ρ, while the same increase in P required roughly a factor of two increase in T. Thus for the comparisons presented here, T is a more appropriate second variable to equate than ρ. We therefore chose to fix the T in the FT-DFT simulations and vary the ρ until the experimentally inferred P was reached.

The resulting P, T, and ρ states obtained in this way using PBE, vdW-DF1, and vdW-DF2 xc functionals are listed in Table II (for each functional P and T are the same as those listed under Kerley03). As expected, systematic differences

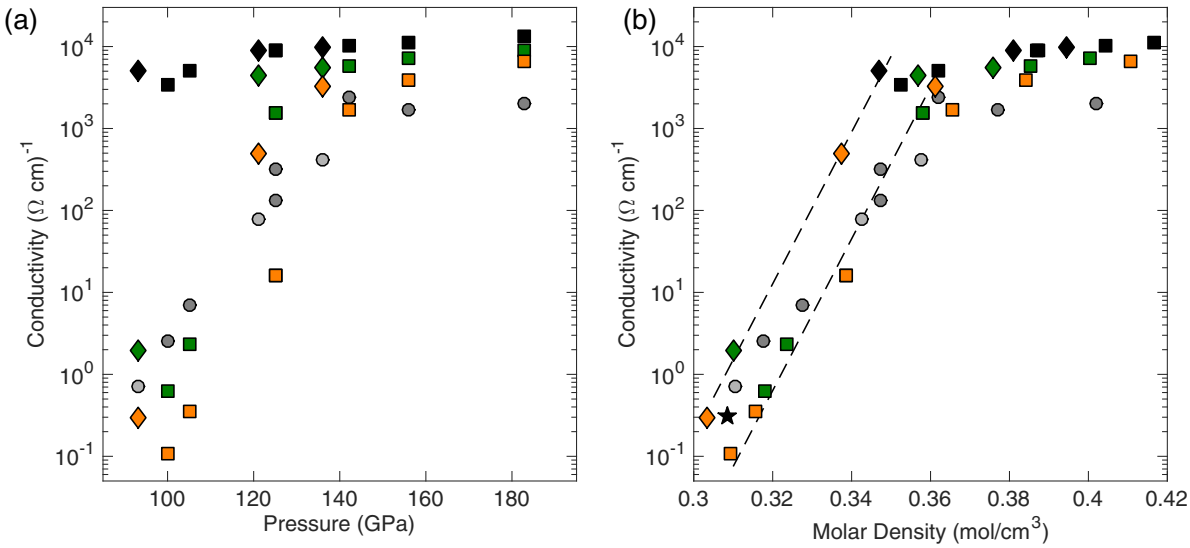

FIG. 5. Conductivity as a function of (a) P and (b) molar density. Dark (light) gray circles, measured [21,22] σ for hydrogen (deuterium). Black, green, and orange squares (diamonds), calculated σ of hydrogen (deuterium) using PBE [8], vdW-DF1 [9], and vdW-DF2 [10] xc functionals, respectively, at the conditions listed in Table II. The black star is an additional calculated conductivity using PBE at a lower molar density described in Sec. IV. Dashed lines in (b) are guides to the eye that are offset by one order of magnitude in σ.

in the inferred ρ were observed. In particular, the ρ inferred using the PBE xc functional were found to be significantly larger (∼9–12%) than the values obtained from Kerley03. In contrast, both of the nonlocal vdW xc functionals resulted in ρ values that were in better agreement with the Kerley03 EOS. For both functionals the ρ was found to be lower than Kerley03 at low P (−0.1% and −2.2% for vdW-DF1 and vdW-DF2, respectively) and higher than Kerley03 at high P (+5.4% and +2.1% for vdW-DF1 and vdW-DF2, respectively). These ρ differences and their effect on the calculated σ will be discussed in more detail in the next section.

The calculated σ for the various xc functionals at these P, T, and ρ conditions are listed in Table II and plotted as a function of P in Fig. 5(a). This comparison suggests that PBE significantly overestimates σ in this P, T, and ρ regime. In particular, calculations using the PBE xc functional predict that a minimum metallic conductivity should have been observed in all experiments performed by NWM. In contrast, the overall trend of the experimental data is captured reasonably well by the two nonlocal vdW functionals. However, when σ is plotted as a function of molar density, as in Fig. 5(b), all three functionals appear to adequately reproduce the experimental results. In particular, the predicted σ for the two sets of calculations (hydrogen and deuterium) collapse onto linear trend lines in $\log(\sigma)$ vs ρ (dashed lines in Fig. 5). These trend lines are systematically offset by one order of magnitude in σ. We note that given the higher shock impedance of deuterium, those experiments reached ∼400 K higher T at a similar P and molar density as compared to hydrogen. These isotopic differences will be explored further in the next section.

Similar behavior is exhibited in the inferred energy gaps extracted from FP calculations of the DOS. Figure 6 shows the calculated DOS for the conditions reached in the subset of hydrogen experiments performed by NWM. Energy gap values obtained for the various xc functionals at the T and ρ conditions listed in Table II are plotted in Fig. 7 as functions of both P and molar density. Also shown in the figure for reference are the inferred energy gap values obtained from the measured σ using Eq. (1) with $\sigma_0 = 1850\ (\Omega\,\mathrm{cm})^{-1}$ and the T and ρ values inferred from the Kerley03 EOS. As was the case for σ, PBE appears to significantly underestimate the energy gap in this P, T, and ρ regime, while the nonlocal vdW functionals are in reasonable agreement with the energy gap values inferred from the simple semiconductor model described in Sec. II. However, again, when viewed as a function of molar density, all three functionals appear to exhibit very similar results; the extracted energy gaps for the two sets of calculations (hydrogen and deuterium) collapse onto linear trend lines (dashed lines in Fig. 7). These trend lines are offset in energy, with the deuterium trend line being systematically ∼1 eV lower than that of hydrogen. Again, these isotopic differences will be explored further in the next section.

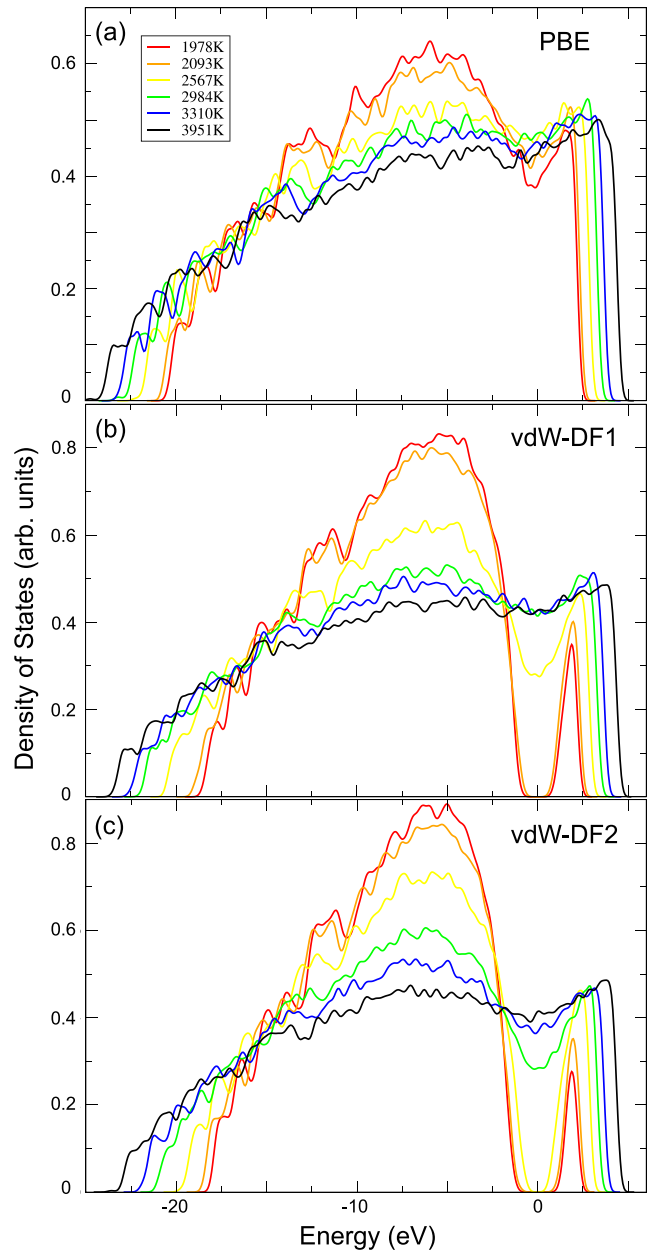

FIG. 6. Density of states extracted from FP calculations for (a) PBE, (b) vdw-DF1, and (c) vdW-DF2 at the P, T, and ρ conditions (listed in Table II) reached in the multiple-shock experiments [21,22] on hydrogen performed by NWM.

IV. DISCUSSION

The comparisons shown in Figs. 5 and 7 suggest that the most important parameter in determining the location of the MA transition for the various xc functionals is the molar density, at least in this P, T, and ρ regime. Given this observation, and the significantly larger ρ predicted by PBE at the P and T conditions considered here, one must ask the question whether the comparison of the NWM experiments with PBE is biased by our choice to equate the P and T in the peak state as opposed to the P and ρ. To investigate this we performed several more FP calculations of experiment SLDMS13-H_2 (one of the lower P hydrogen experiments) using the PBE xc functional.

Fixing the T and ρ at 2093 K and 0.66 g/cm^3 (conditions estimated by the Kerley03 EOS) results in a P of 88 GPa for the PBE xc functional, ∼16% lower than the experimentally inferred P of 105 GPa. An increase of ∼10%

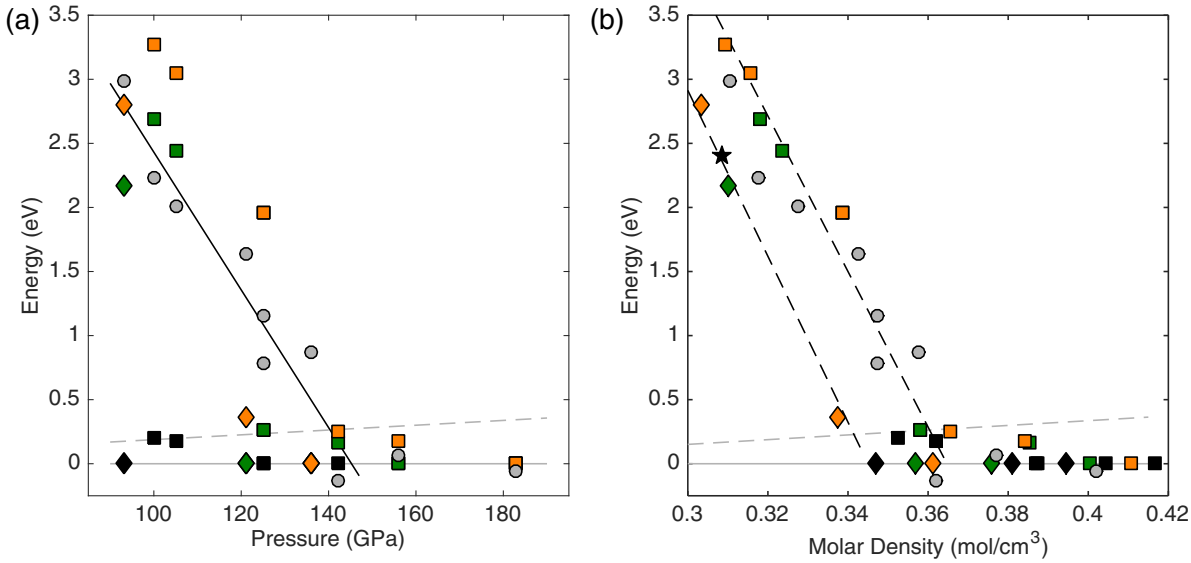

FIG. 7. Energy gap as a function of (a) P and (b) molar density. The gray circles are the energy gap values obtained from Eq. (1) using $\sigma_0 = 1850\ (\Omega\ \mathrm{cm})^{-1}$ with the T and ρ values inferred from the Kerley03 [28] EOS (see Table II). The dashed gray line denotes the temperature of the system in eV ($k_B T$ as a function of P or ρ); the solid black line is a fit to data where the inferred gap was greater than the temperature of the system. Black, green, and orange squares (diamonds), calculated energy gap of hydrogen (deuterium) using PBE [8], vdW-DF1 [9], and vdW-DF2 [10] xc functionals, respectively, at the conditions listed in Table II. The black star is an additional calculated energy gap using PBE at a lower molar density described in Sec. IV. Dashed lines in (b) are guides to the eye and indicate an offset of ∼1 eV between hydrogen and deuterium.

in ρ (to 0.729 g/cm^3) was required to increase the P to 105 GPa. These were the P, T, and ρ values used in the calculations described in the previous section (see Table II). Here, we instead fixed the ρ at 0.66 g/cm^3 and varied the T. A T increase to 5800 K (a factor of ∼2.8) was required to match the experimentally inferred P of 105 GPa. The resulting state was found to exhibit metallic behavior, with $\sigma = 7500\ (\Omega\ \mathrm{cm})^{-1}$ and no energy gap. We performed a similar exercise at an intermediate ρ of 0.689 g/cm^3. In this case, a T increase to 4200 K (a factor of ∼2) was required to reach the experimentally inferred P of 105 GPa. Again, this state was found to exhibit metallic behavior, with $\sigma = 7600\ (\Omega\ \mathrm{cm})^{-1}$ and no energy gap. It seems clear that for the PBE xc functional no matter what T and ρ combination one uses to match the experimentally inferred P of 105 GPa, the calculated σ will be much too high, by roughly three orders of magnitude. The same conclusions would be reached for the higher P experiments performed by NWM. From this exercise we conclude that regardless of how one tries to equate the P states reached in the NWM experiments, predictions using the PBE xc functional are inconsistent with the measured σ.

To further explore the trends observed in σ and energy gap with molar density, we also performed calculations with the PBE xc functional at lower P. The Kerley03 EOS was used to estimate the T that would be reached in a ∼ 80 GPa multiple-shock experiment. These P and T conditions, 80 GPa and 1500 K, respectively, correspond to a molar density of 0.3085 g/cm^3 with the PBE xc functional. At these conditions PBE predicts $\sigma = 0.31\ (\Omega\ \mathrm{cm})^{-1}$ and an energy gap of 2.4 eV [shown as black stars in Figs. 5(b) and 7(b)]. While these results do reasonably follow the trends exhibited by the nonlocal vdW xc functionals, PBE does appear to display gap closure at a slightly lower molar density. However, we note the T for this PBE calculation is considerably lower (1500 K) than the other calculations considered here.

To evaluate the relative effect of T on the FP calculations we consider σ as a function of band gap energy, shown in Fig. 8. The as calculated values (listed in Table II) are plotted in Fig. 8(a). Also plotted as triangles and squares are the experimentally measured σ as a function of inferred energy gap as determined by NWM and reanalyzed in this work, respectively; dark and light gray correspond to hydrogen and deuterium, respectively. As expected, the FP calculations, particularly with the nonlocal vdW xc functionals, are in reasonable agreement with the experimental measurements and the reanalyzed energy gaps, showing a small scatter about a common trend line. These σ values were then normalized to a common T of 1978 K (the lowest inferred experimental T) using the semiconductor model:

$$\sigma_n = \sigma_1 \exp\left[\frac{-E_{g_1}}{2k_B T_1}\left(\frac{T_1}{1978} - 1\right)\right], \tag{5}$$

where σ_1 at T_1 and E_{g_1} has been normalized to σ_n at T of 1978 K and the same energy gap E_{g_1}. The normalized experimental and calculated σ_n are plotted as a function of energy gap in Fig. 8(b). We see that the small scatter apparent in Fig. 8(a) can be explained by the corresponding T differences. In particular, the low value for σ obtained for the 1500 K PBE calculation is largely due to the correspondingly low thermal excitation. These results do suggest a small isotopic difference for FP calculations of hydrogen and deuterium; σ for deuterium appears to be systematically lower than that of hydrogen by a factor of 2–3. While the source of this small isotopic difference is not entirely clear, it suggests the energy gap is both a function of T and ρ in this regime, as one might expect.

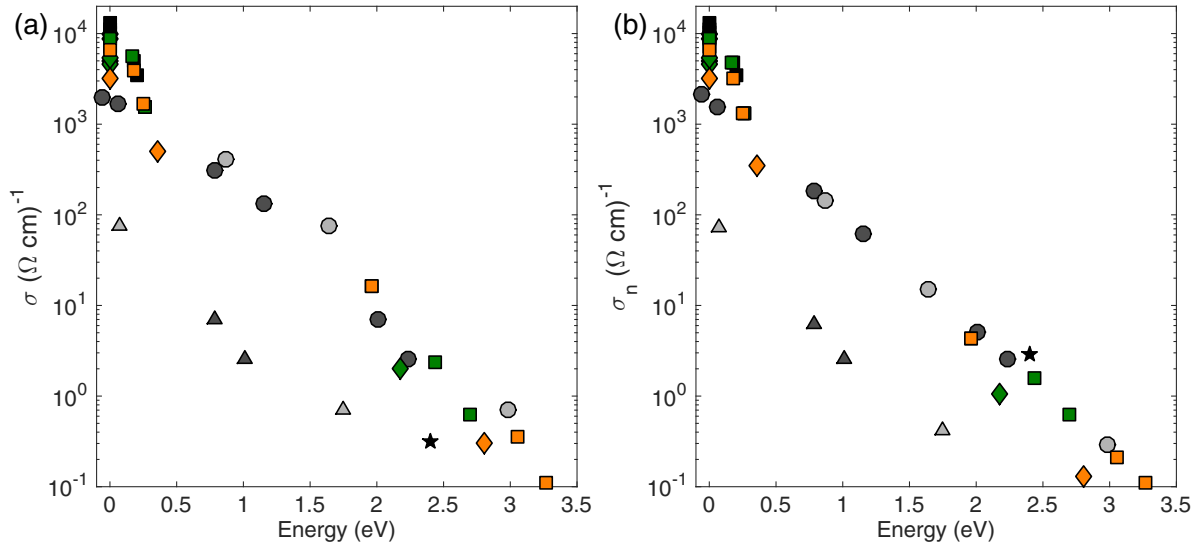

FIG. 8. Conductivity as a function of energy gap. (a) Dark and light gray circles (triangles) are the results for hydrogen and deuterium, respectively, from experiments [21,22] performed by NWM where the energy gap was inferred from the modified (original) semiconductor model described in Sec. II. Black, green, and orange squares (diamonds) are calculations for hydrogen (deuterium) using PBE [8], vdW-DF1 [9], and vdW-DF2 [10] xc functionals, respectively, at the conditions listed in Table II. The black star is the additional PBE calculation performed at lower molar density. (b) Same as (a) but with the conductivity values normalized [Eq. (5)] to a common T (1978 K, corresponding to the lowest T NWM experiment) as described in the text.

These comparisons suggest that the significant differences in σ and the energy gap exhibited by the various xc functionals when viewed as a function of P, as in Figs. 5(a) and 7(a), are largely tied to differences in the predicted P for the xc functionals at similar T and ρ conditions. We note that the various functionals considered here have recently been carefully evaluated with respect to quantum Monte Carlo (QMC) calculations by Clay *et al.* [46]. They explored the accuracy of the various functionals in comparison to QMC calculations for both liquid and solid hydrogen structures. The vdW functionals, particularly vdW-DF1, were found to provide a very good description of the global and local energetics as compared to QMC but exhibited larger differences in P than PBE relative to the QMC calculations. The P obtained from all of the xc functionals were higher than QMC (by ∼5–10% in the relevant ρ regime), with PBE and vdW-DF2 being the lowest and highest, respectively.

This trend in P differences observed by Clay *et al.*, which is consistent with the trend observed in this study, would seem to suggest that the P determined by the vdW functionals is too high rather than the P determined by PBE being too low. However, this conclusion is refuted by the incompatibility of PBE with the measured σ from the NWM experiments. We note that the calculations by Clay *et al.* were carried out in liquid structures with Wigner-Seitz radii (r_s) of 1.30, 1.45, and 1.60 (1.23, 0.88, and 0.66 g/cm^3 in hydrogen, respectively) at $T = 1000$ K. The ρ range considered here corresponds to an r_s of 1.5–1.6, within the range evaluate by Clay *et al.*, however, the T range considered here (2–4 kK) is higher. At higher T, thermal population of electrons into the excited states is not insignificant. This thermal occupation of electronic orbitals has direct consequences on the liquid structure and the forces but is not included in the QMC calculations.

Similar observations were made in a recent evaluation of the various xc functionals with high-precision Hugoniot and reshock measurements on liquid deuterium [7], which probed the MA transition in the largely T-driven regime. In that study the same trend in P was observed for the MA transition along the principal Hugoniot; dissociation, as evidenced by a transient drop in the slope of the shock velocity relative to the particle velocity behind the shock front, occurred at a lower P for PBE than for the vdW functionals. Furthermore, the experimentally determined P onset of dissociation was found to be bounded from below by PBE (∼3 GPa lower than experiment) and above by the vdW functionals (∼1 GPa higher than experiment). This conclusion was corroborated by measurements of the reshock P from Hugoniot states near peak compression. Those measurements suggest that the reshock P determined by the vdW functionals are too low by a few percent. In contrast, the P difference for vdW-DF1 relative to QMC at those conditions is on the order of +2–4%. Again, while the trend in P was found to be the same as that determined by Clay *et al.*, comparison with the MA transition along the Hugoniot suggests that the P for dissociation is in better agreement with the vdW xc functionals and that PBE underestimates the P necessary for dissociation.

Finally, we note that there are conflicting experimental results for the MA transition in the low-T, high-ρ regime where the transition appears to be largely ρ driven (see Fig. 1). Dynamic compression experiments [15] on liquid deuterium in the ∼1–2 kK regime performed at the Sandia Z machine revealed an abrupt MA transition, as evidenced by a rapid increase in reflectivity, between ∼280 and 305 GPa. Similar to the T-driven regime probed by the Hugoniot and the intermediate regime probed by the σ measurements of NWM, the dynamic compression experimental results are in

reasonable agreement with the nonlocal vdW xc functionals and suggest that the PBE xc functional underestimates the P onset of the MA transition. In contrast, static high-P and pulsed heated experiments [17–20] on hydrogen and deuterium in a similar T regime suggest the MA transition occurs at ∼75 to 170 GPa, based on observation of T plateaus in the heating curves and increases in reflectivity, in apparent agreement with PBE. However, these conditions are consistent with the onset of strong optical absorption in the dynamic compression experiments, which lead to alternative interpretations of those data [11,15,47]. Furthermore, we have shown that the predictions of PBE are inconsistent with the σ measurements of NWM. This raises questions about the static high-P and pulsed heated studies, particularly given that the MA transition in those studies is reported to be in a very similar P but even lower T range than the multiple-shock σ experiments examined here.

V. CONCLUSION

A detailed comparison of the measured σ from multiple-shock compression experiments [21,22] with FT-DFT calculations using both semilocal (PBE) and nonlocal (vdW-DF1 and vdW-DF2) xc functionals was performed. As a part of this comparison, the multiple-shock σ experiments were reanalyzed; the original study included inconsistencies in both the inferred T states reached in the experiments and in the fit to a semiconductor model used to interpret the measured σ. Due to the method used to infer the T, which only accounted for the entropy increase from the first shock and treated subsequent compression as isentropic, the T states reported by NWM are systematically low by ∼440–750 K (∼20–30%). Also, due to a low $\sigma_0 = 90\ (\Omega\ \mathrm{cm})^{-1}$, the energy gap inferred from a simple semiconductor model is underestimated by ∼1 eV as a function of P as compared to the same semiconductor model with a more reasonable $\sigma_0 = 1850\ (\Omega\ \mathrm{cm})^{-1}$.

Using P and T conditions inferred from the Kerley03 EOS for the peak states, FP calculations with PBE, vdW-DF1, and vdW-DF2 xc functionals were performed to directly compare with the NWM experiments. Calculations of σ using the PBE xc functional predict that a minimum metallic conductivity should have been observed in all of the experiments performed by NWM. It was also shown that regardless of how one tries to equate the P states reached in the NWM experiments, predictions using the PBE xc functional are inconsistent with the measured σ. In contrast, the overall trend of the experimental data is captured reasonably well by the two vdW xc functionals. Similar behavior was exhibited in the inferred energy gaps extracted from FP calculations of the DOS.

This study, along with previous studies comparing the various xc functionals with recent Hugoniot experiments [7] on deuterium that probed the MA transition in the high-T and low-ρ regime and dynamic compression experiments [15] on deuterium that probed the MA transition in the low-T and high-ρ regime, provides a consistent picture for the MA transition over a wide P and T range. Over this entire range the P onset of the MA transition is captured reasonably well by the nonlocal vdW xc functionals, while PBE appears to underestimate the P conditions necessary for dissociation. This likely stems from P errors associated with the PBE xc functional, resulting in calculated P that are too low at these T and ρ conditions. This raises questions about recent static high-P and pulsed heated studies [17–20] that appear to be in agreement with predictions from PBE, particularly given that the MA transition in those studies is reported to be in a very similar P but even lower T range than the multiple-shock σ experiments examined here.

ACKNOWLEDGMENTS

This work was supported in part by the US Department of Energy, National Nuclear Security Administration under Award No. DE-NA0002007. Sandia National Laboratories is a multimission laboratory managed and operated by National Technology and Engineering Solutions of Sandia, LLC., a wholly owned subsidiary of Honeywell International, Inc., for the US Department of Energy's National Nuclear Security Administration under Contract No. DE-NA0003525. This paper describes objective technical results and analysis. Any subjective views or opinions that might be expressed in the paper do not necessarily represent the views of the US Department of Energy or the United States Government. M.P. and R.R. thank the Deutsche Forschungsgemeinschaft (DFG) for support via the SFB 652.

[1] J. M. McMahon, M. A. Morales, C. Pierleoni, and D. M. Ceperley, Rev. Mod. Phys. **84**, 1607 (2012).
[2] R. Smoluchowski, Nature (London) **215**, 691 (1967).
[3] E. E. Salpeter, Astrophys. J. **181**, L83 (1973).
[4] W. Lorenzen, B. Holst, and R. Redmer, Phys. Rev. B **84**, 235109 (2011).
[5] T. Guillot, Science **286**, 72 (1999).
[6] N. Nettelmann, A. Becker, B. Holst, and R. Redmer, Astrophys. J. **750**, 52 (2012).
[7] M. D. Knudson and M. P. Desjarlais, Phys. Rev. Lett. **118**, 035501 (2017).
[8] J. P. Perdew, K. Burke, and M. Ernzerhof, Phys. Rev. Lett. **77**, 3865 (1996).
[9] M. Dion, H. Rydberg, E. Schröder, D. C. Langreth, and B. I. Lundqvist, Phys. Rev. Lett. **92**, 246401 (2004).
[10] K. Lee, E. D. Murray, L. Kong, B. I. Lundqvist, and D. C. Langreth, Phys. Rev. B **82**, 081101 (2010).
[11] I. Tamblyn and S. A. Bonev, Phys. Rev. Lett. **104**, 065702 (2010).
[12] M. A. Morales, C. Pierleoni, E. Schwegler, and D. M. Ceperley, Proc. Natl. Acad. Sci. USA **107**, 12799 (2010).
[13] W. Lorenzen, B. Holst, and R. Redmer, Phys. Rev. B **82**, 195107 (2010).
[14] M. A. Morales, J. M. McMahon, C. Pierleoni, and D. M. Ceperley, Phys. Rev. Lett. **110**, 065702 (2013).
[15] M. D. Knudson, M. P. Desjarlais, A. Becker, R. W. Lemke, K. R. Cochrane, M. E. Savage, D. E. Bliss, T. R. Mattsson, and R. Redmer, Science **348**, 1455 (2015).
[16] M. K. Matzen, M. A. Sweeney, R. G. Adams, J. R. Asay, J. E. Bailey, G. R. Bennett, D. E. Bliss, D. D. Bloomquist, T. A.

Brunner, R. B. Campbell, G. A. Chandler, C. A. Coverdale, M. E. Cuneo, J.-P. Davis, C. Deeney, M. P. Desjarlais, G. L. Donovan, C. J. Garasi, T. A. Haill, C. A. Hall, D. L. Hanson, M. J. Hurst, B. Jones, M. D. Knudson, R. J. Leeper, R. W. Lemke, M. G. Mazarakis, D. H. McDaniel, T. A. Mehlhorn, T. J. Nash, C. L. Olson, J. L. Porter, P. K. Rambo, S. E. Rosenthal, G. A. Rochau, L. E. Ruggles, C. L. Ruiz, T. W. L. Sanford, J. F. Seamen, D. B. Sinars, S. A. Slutz, I. C. Smith, K. W. Struve, W. A. Stygar, R. A. Vesey, E. A. Weinbrecht, D. F. Wenger, and E. P. Yu, Phys. Plasmas **12**, 055503 (2005).

[17] V. Dzyabura, M. Zaghoo, and I. F. Silvera, Proc. Natl. Acad. Sci. USA **110**, 8040 (2013).

[18] K. Otha, K. Ichimaru, M. Einaga, S. Kawaguchi, K. Shimizu, T. Matsuoka, N. Hirao, and Y. Ohishi, Sci. Rep. **5**, 16560 (2015).

[19] M. Zaghoo, A. Salamat, and I. F. Silvera, Phys. Rev. B **93**, 155128 (2016).

[20] M. Zaghoo and I. F. Silvera, Proc. Nat. Acad. Sci. USA **114**, 11873 (2017).

[21] S. T. Weir, A. C. Mitchell, and W. J. Nellis, Phys. Rev. Lett. **76**, 1860 (1996).

[22] W. J. Nellis, S. T. Weir, and A. C. Mitchell, Phys. Rev. B **59**, 3434 (1999).

[23] A. C. Mitchell and W. J. Nellis, Rev. Sci. Instrum. **52**, 347 (1981).

[24] G. I. Kerley, *Molecular-based study of fluids* (American Chemical Society, Washington, 1983), p. 107.

[25] N. C. Holmes, M. Ross, and W. J. Nellis, Phys. Rev. B **52**, 15835 (1995).

[26] M. Ross, Phys. Rev. B **54**, R9589 (1996).

[27] M. Ross, Phys. Rev. B **58**, 669 (1998).

[28] G. Kerley, Sandia National Laboratories Report No. SAND2003-3613 (Sandia National Laboratories, 2003).

[29] J. H. Carpenter (private communication, 2014).

[30] K. R. Cochrane, R. W. Lemke, Z. Riford, and J. H. Carpenter, J. Appl. Phys. **119**, 105902 (2016).

[31] G. I. Kerley, Int. J. Impact Eng. **5**, 441 (1987).

[32] G. Kerley, Kerley Publishing Services Report No. KPS98-1 (Kerley Publishing Services, 1998).

[33] J. F. Barnes and S. P. Lyon, Los Alamos Technical Report No. LA-11058-MS (Los Alamos National Laboratory, 1987).

[34] D. Saumon (private communication, 2018).

[35] L. Caillabet, S. Mazevet, and P. Loubeyre, Phys. Rev. B **83**, 094101 (2011).

[36] B. Holst, R. Redmer, and M. P. Desjarlais, Phys. Rev. B **77**, 184201 (2008).

[37] G. Kresse and J. Hafner, Phys. Rev. B **47**, 558 (1993).

[38] G. Kresse and J. Hafner, Phys. Rev. B **49**, 14251 (1994).

[39] G. Kresse and J. Furthmüller, Phys. Rev. B **54**, 11169 (1996).

[40] S. Nosé, Mol. Phys. **52**, 255 (1984).

[41] S. Nosé, J. Chem. Phys. **81**, 511 (1984).

[42] W. G. Hoover, Phys. Rev. A **31**, 1695 (1985).

[43] R. Kubo, J. Phys. Soc. Jpn. **12**, 570 (1957).

[44] D. A. Greenwood, Proc. Phys. Soc. **71**, 585 (1958).

[45] H. J. Monkhorst and J. D. Pack, Phys. Rev. B **13**, 5188 (1976).

[46] R. C. Clay, J. Mcminis, J. M. McMahon, C. Pierleoni, D. M. Ceperley, and M. A. Morales, Phys. Rev. B **89**, 184106 (2014).

[47] R. S. McWilliams, D. A. Dalton, M. F. Mahmood, and A. F. Goncharov, Phys. Rev. Lett. **116**, 255501 (2016).